Jagiellonian University in Kraków
Faculty of Physics, Astronomy and Applied Computer Science

Kryshtal Pavlo

Album number: 1157712

Investigation of the sputtering process of two-dimensional samples made of hexagonal boron nitride with C_{60} projectiles

Master's thesis

in the specialization Advanced Materials and Nanotechnology

under the supervision of
prof. dr. hab. Zbigniewa Postawy
Department of Physics of Nanostructures and Nanotechnology

Kraków 2020

Oświadczenie autora pracy

Świadom odpowiedzialności prawnej oświadczam, że niniejsza praca dyplomowa została napisana przeze mnie samodzielnie i nie zawiera treści uzyskanych w sposób niezgodny z obowiązującymi przepisami.
Oświadczam również, że przedstawiona praca nie była wcześniej przedmiotem procedur związanych z uzyskaniem tytułu zawodowego w wyższej uczelni.

Kraków, dnia Podpis autora pracy

Oświadczenie kierującego pracą

Potwierdzam, że niniejsza praca została przygotowana pod moim kierunkiem i kwalifikuje się do przedstawienia jej w postępowaniu o nadanie tytułu zawodowego.

Kraków, dnia Podpis kierującego pracą

I would like to express my great appreciation to Prof. dr hab. Zbigniew Postawa for his valuable and constructive suggestions during the planning and development of this research work. His willingness to give his time so generously is very much appreciated.

I am grateful to Ph.D. students of the research group for support and a nice atmosphere.

Contents

Wstęp

Spektrometria mas jonów wtórnych (SIMS) jest szeroko stosowaną metodą analizy składu chemicznego powierzchni różnych materiałów. W tej technice powierzchnia próbki jest bombardowana przez wiązkę jonów, a wyrzucane jony wtórne są zbierane i analizowane w spektrometrach masowych. Stosunek masy do ładunku jonów wtórnych dostarcza informację o składzie pierwiastkowym, izotopowym lub molekularnym powierzchni. SIMS umożliwia detekcję prawie wszystkich pierwiastków chemicznych. Jednak analiza związków organicznych, w szczególności monowarstw organicznych, jest trudna. Głównym problemem występującym w tym przypadku jest zbyt słaby sygnał SIMS. Kilka lat temu zaproponowano nową konfigurację metody SIMS w celu zwiększenia wydajności wykrywania rozpylanych jonów [1]. W tej konfiguracji pocisk uderza od spodu w ultra-cienkie podłoże i rozpyla osadzony na nim analizowany materiał bezpośrednio w kierunku detektora. Co więcej, kilku autorów pokazało, że obecność podłoża grafenowego prowadzi do wzrostu wydajności ujemnej jonizacji molekuł organicznych w tej konfiguracji SIMS [1]. Dotychczasowe badania przeprowadzono z wielowarstwowymi podłożami grafenowymi [2], jednak poziom sygnału wciąż może być niewystarczający w wymagających eksperymentach, dlatego poszukiwanie innych materiałów na ultra-cienkie podłoża jest wciąż aktualne.

Dlatego celem niniejszej pracy jest modelowanie procesu rozpylania jednowarstwowych podłoży grafenu i h-BN, oraz porównanie wydajności rozpylania dla tych podłoży, zmierzonych w tych samych warunkach. Głównym celem pracy jest ocena perspektyw użycia tych podłoży w badaniach SIMS dla niewielkich ilości materiałów organicznych. Obydwa podłoża mają podobną strukturę geometryczną (tzw. struktura plastra miodu), ale różnią się właściwościami sprężystymi i energiami wiązania atomów.

Symulacje zostały przeprowadzone za pomocą metody dynamiki molekularnej z wykorzystaniem programu do symulacji - LAMMPS [3].

1. Introduction

Nowadays, secondary ion mass spectrometry (SIMS) is widely used for the analysis of the chemical composition of surfaces of various materials. In this technique, the surface under study is sputtered with a focused ion beam, and ejected secondary ions are collected and analyzed by mass spectrometers. The mass to charge ratios of the secondary ions provide information on the elemental, isotopic, or molecular composition of the surface. SIMS can perfectly analyze almost all chemical elements, however, the analysis of organic compounds, especially monolayers, meet difficulties. The major problem is a too weak signal in this case. Recently, a new configuration of the SIMS method has been developed to increase the efficiency of the detection of sputtered ions [1]. In this configuration, a projectile impacts at the bottom of the ultra-thin substrate and sputters the analyzed material deposited on this substrate directly towards the detector. Furthermore, several authors report that a presence od graphene substrate leads to an increase in the ionization efficiency of organic molecules in this SIMS configuration [1]. Early experiments were carried out with multilayers graphene substrates [2], however, the signal level still can be insufficient in demanding experiments, and the quest for other substrates is up to date.

Therefore, the objective of the current work is the simulation of the sputtering process of graphene and h-BN single layer substrates and comparison of the sputtering yields of both these substrates under the same bombardment conditions. We aimed to assess the prospects of these substrates for SIMS studies of tiny amounts of organic materials. Both substrates have similar honeycomb structure but differ in elastic properties and binding energies of atoms.

The simulations were carried out by methods of molecular dynamics using a Large-scale Atomic/Molecular Massively Parallel Simulator (LAMMPS) [3].

2. Literature overview

2.1. Secondary ion mass spectrometry (SIMS)

Secondary ion mass spectrometry (SIMS) is a microanalytical technique for secondary ions detection, which were sputtered from a surface sample by high-energy primary ions of the beam [4]. SIMS can analyze almost all elements from hydrogen to uranium and is widely used in modern science.

Fig. 2.1 shows a block diagram of a secondary ion mass spectrometer after [4]. The basis of SIMS is to utilize a focused ion beam to erode atoms from a selected area of a sample surface. The primary beam can be composed of various ions, typically having the energy in the range of 0.5-50 keV. A charged portion of the eroded atoms is extracted via an electrical potential and subsequently analyzed by energy a mass spectrometer. Electron multiplier and Faraday cup can be used in the detection module.

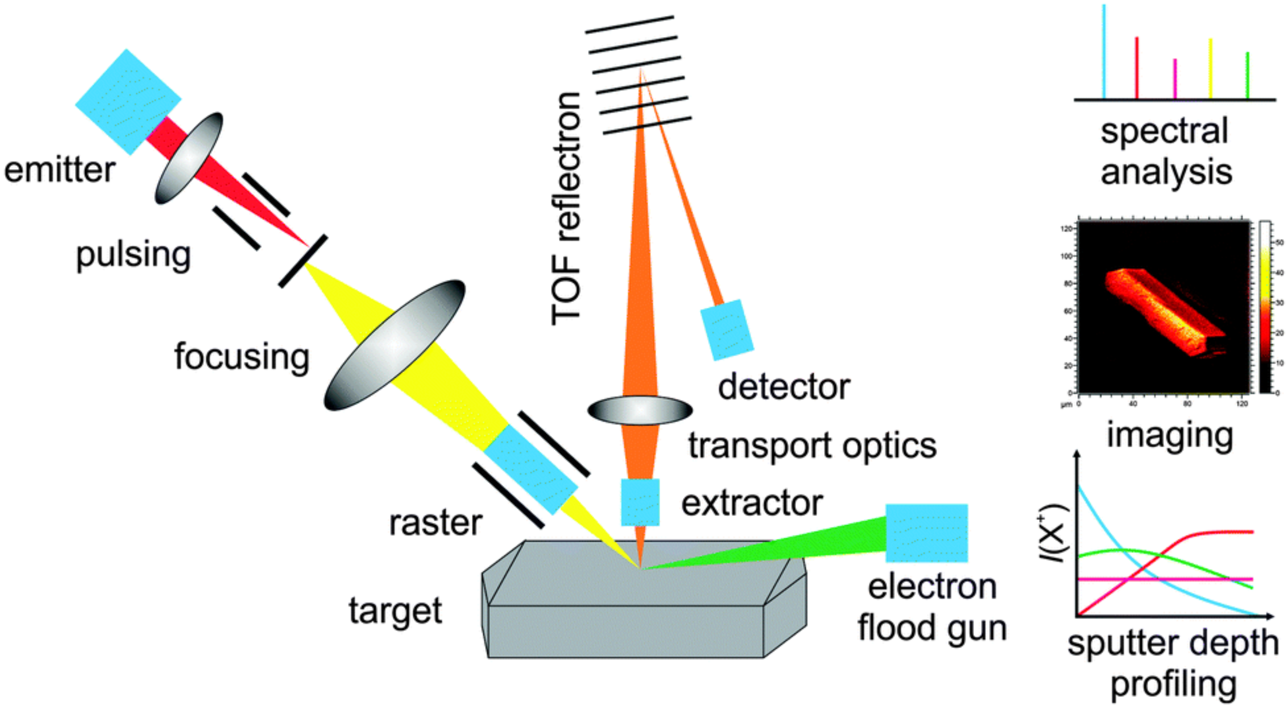

Fig.2.1 Block diagram of Secondary Ion Mass Spectrometer [5].

The image in fig 2.1 presents one of the SIMS configurations. It should be noted that high spatial resolution results in a relatively low analytical precision and vice versa [6].

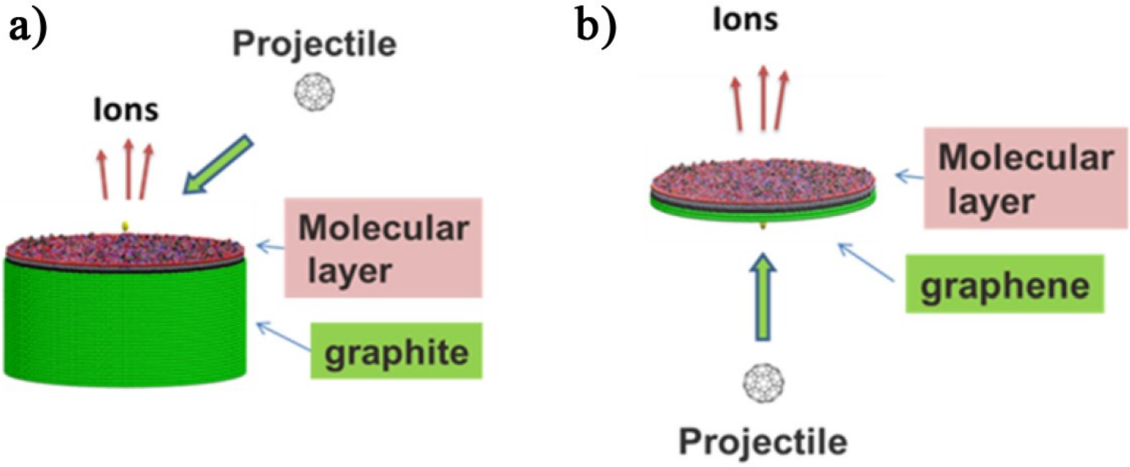

Fig. 2.2. Graphical representation of two experimental layouts of SIMS [1].

In the case of organic layers studies, two experimental configurations are used in SIMS (fig. 2.2). The first configuration, which is a classical one, uses a massive substrate covered with a layer of an organic compound. Both projectile and detector are located above the substrate. The second configuration uses a thin substrate covered with organic material [3]. The projectile is located under the substrate and sputters it towards the detector, significantly improving the sputtering efficiency and SIMS signal [3]. This is mainly due to the indirect interaction of the projectile with the organic layer [3]. Furthermore, due to the small thickness of the support layer, which results in a small amount of sputtered substrate material, the fraction of the organic molecules dominates in the analyzed signal [7].

2.2 Molecular Dynamics Computer Simulations

Molecular dynamics simulation is based on the analysis of the movements of atoms and molecules [8]. It is Newton's equations of motion, which should be solved for a system of interacting particles using various interatomic potentials. LAMMPS program was used for solving the equations [3].

Molecular dynamics simulations are an essential complementary technique to the conventional experiments, enabling one to significantly reduce costs of the later or even perform simulations in the conditions which are hardly reachable in practice. On the other hand, principal simulation results should be verified and confirmed experimentally to avoid faulty judgments and conclusions.

2.3 Potentials

Simulations with methods of molecular dynamics require a clear definition of interactions between atoms in the system under study. These interactions are typically described with a potential function. There are plenty of potentials already developed. Utilization of a potential or combination of several potentials enables one to simulate even complicated systems. The potentials, which were used in the present work, are described below.

2.3.1 BN-EXTEP potential

The BN-EXETEP is a many-body potential, which is an improved version of a classic Tersoff potential with a correction to the bond order [9]. This correction enabled one to distinguish situations where the coordination numbers are identical, but chemical elements are not the same. The total energy of the system is described in the form:

$$E = \frac{1}{2}\sum_{ij} fc(r_{ij})\left[V_R(r_{ij}) - B_{ij}V_A(r_{ij})\right], \tag{2.1}$$

where r_{ij} is the interatomic distance, V_A and V_R are attractive and repulsive potentials, respectively. The double sum runs all i and j atoms, and cutoff function of f is described in the form [9]:

$$f_C(r) = \begin{cases} 1 & r \leq R - D \\ \frac{1}{2}\left[1 - sin\left(\frac{\pi(r-R)}{2D}\right)\right] & |R - r| < D\,, \\ 0 & r\ \geq R + D \end{cases} \tag{2.2}$$

where R and D are distance units.

The implementation of a complete BN-EXTEP potential in LAMMPS software [3] enabled large-scale molecular dynamics simulations of BN based systems.

The BN-EXTEP potential was used for describing B-N interactions in the BN substrate in the current study.

2.3.2 ZBL potential

The ZBL (Ziegler-Biersack-Littmark) is a pair-wise potential, which is primarily used for describing collisions of high energy atoms [10]. The ZBL potential accurately describes repulsive interactions due to parameterization by the quantum mechanics methods. The mathematical description of ZBL potential E_{ij}^{ZBL} is given by:

$$E_{ij}^{ZBL} = \frac{1}{4\pi\epsilon_0}\frac{Z_i Z_j e^2}{r_{ij}}\phi\left(\frac{Z_i^{0.23} + Z_j^{0.23}}{0.46850}r_{ij}\right) + S(r_{ij}), \qquad (2.3)$$

where electron charge is e, Z_i and Z_j are atomic numbers of the atom i $and j$, the electric permeability of the vacuum is ϵ_0, $\phi(x)$ is a parameterized function, $S(r_{ij})$ – is switching function, which is intended to ramp smoothly to zero the force, energy, and curvature between an inner and outer cutoff.

The ZBL potential was used for describing of C-B and C-N interactions between the projectile and substrate atoms.

2.3.3 AIREBO potential

Many-body potential *Adaptive Intermolecular Reactive Empirical Bond Order* (AIREBO) [11] is a potential, which is used to describe of C-C, C-H, and H-H interactions in hydrocarbons. The AIREBO potential is given by:

$$E = \frac{1}{2}\sum_i \sum_{j\neq i}\left[E_{ij}^{rebo} + E_{ij}^{LJ} + \sum_{k\neq i}\sum_{l\neq i,j,k} E_{kijl}^{torsion}\right], \qquad (2.4)$$

where E^{rebo} is pair-wise REBO[11] hydrocarbon potential, which describes C-C, C-H, and H-H short-range binding, E^{JL} is the Lennard-Jones potential, which describes long-range interaction, $E^{torsion}$ is a four-body potential, which accounts for directivity and saturation bindings in hydrocarbons.

The AIREBO potential was used for describing C-C interactions between atoms of graphene substrate and C_{60} projectile in the current study.

2.3.4 Lennard-Jones potential

The Lennard-Jones (LJ) potential is an interatomic potential, which was created for describing noble gas interactions [12]. Because noble gases have completely filled valence electron shells, they are chemically inert. The mathematical formula for the potential energy V_{LJ}^{ij} between two atoms i and j is given by:

$$V_{LJ}^{ij}(r) = \epsilon\left(\left(\frac{\sigma}{r_{ij}}\right)^{12} - 2\left(\frac{\sigma}{r_{ij}}\right)^{6}\right), \tag{2.5}$$

where ε is the depth of the potential well, σ is the distance at which the potential has a minimum value. The first term of the formula (1) represents electrostatic repulsion of atomic cores and quantum repulsion of electron shells, while the second term describes attraction forces. The primary parameters of the potential are σ and ε. The variation of these parameters leads to a change in the energy of interaction between atoms.

The LJ potential was used for describing long-range interactions in AIREBO potential, which was described in the previous section.

3. Modelled systems

In this study, two systems are investigated, namely (1) the C_{60} – hexagonal BN (h-BN) and (2) C_{60}-graphene. Both systems consist of a single C_{60} projectile and a substrate, which is either a single h-BN or graphene layer. The substrates are sputtered by the C_{60} projectile, which is initially located 15 Å below the substrate, as shown in Figure 3.1.

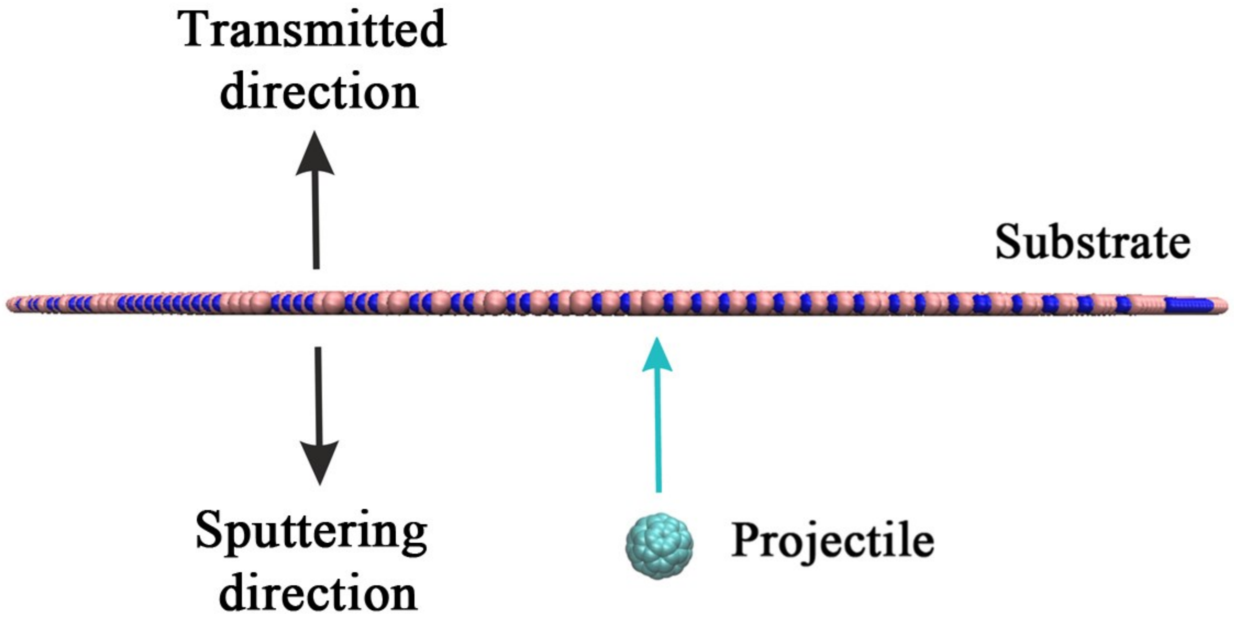

Fig. 3.1. Graphical representation of the h-BN substrate and a C_{60} projectile. B and N substrate atoms are represented by pink and blue colors, respectively. The C atoms of the projectile are represented by turquoise color. The turquoise arrow shows the initial direction of motion of the projectile.

The kinetic energy of the projectile is varied in the range of 0.6 – 50 keV for both substrates. Several impact angles in the range of 0° - 82° are used for every energy point. Such a large variation in the energy and angles was motivated by the quest for finding the optimal values for energy and impact angle in the system under study. Twenty-five points on each substrate were impacted for each kinetic energy and incident angle, and the average number and standard deviation of emitted particles were calculated. It should be noted that all substrate atoms located further than 20 Å above the substrate were considered as emitted. It should be noted that in the simulations, all particles located 5 Å below the substrate, at the final stage of the simulations, were treated and counted as sputtered particles.

3.1 C_{60} cluster

The C_{60} projectile is a fullerene, which consists of 60 carbon atoms (C) connected by single and double bonds with 720 Da total mass. These atoms form a closed shell that resembles a soccer ball and is referred to as Buckminsterfullerene (Fig. 3.2).

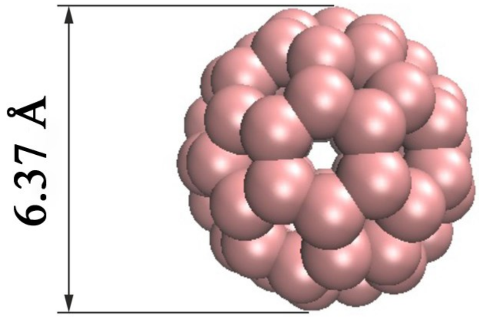

Fig. 3.2. Graphical representation of fullerene C_{60}

C_{60} fullerene molecule was chosen as a projectile in the simulations in the study. The C_{60} projectile has advantages compared to monoatomic projectiles in organic layer sputtering, and its utilization results in a significant increase in organic particle emission [13]. It should be noted that the C_{60} projectile is widely used in the majority of SIMS installations worldwide.

3.2 h-BN and graphene substrates

A single atomic layer of hexagonal boron nitride is used as the substrate (Fig 3.1). The layer has a two-dimensional hexagonal structure with boron and nitride atoms, which form a honeycomb structure. The graphene layer has similar to the h-BN honeycomb structure and cell size, as it is shown in Figure 3.3. The bindings energies for B-N and C-C atoms in single-layer substrates were calculated by the LAMMPS program, and they amounted to 6.66 eV and 7.41 eV, respectively. The Young modulus of graphene and BN monolayer is 1 TPa and 0.865 TPa, respectively[14].

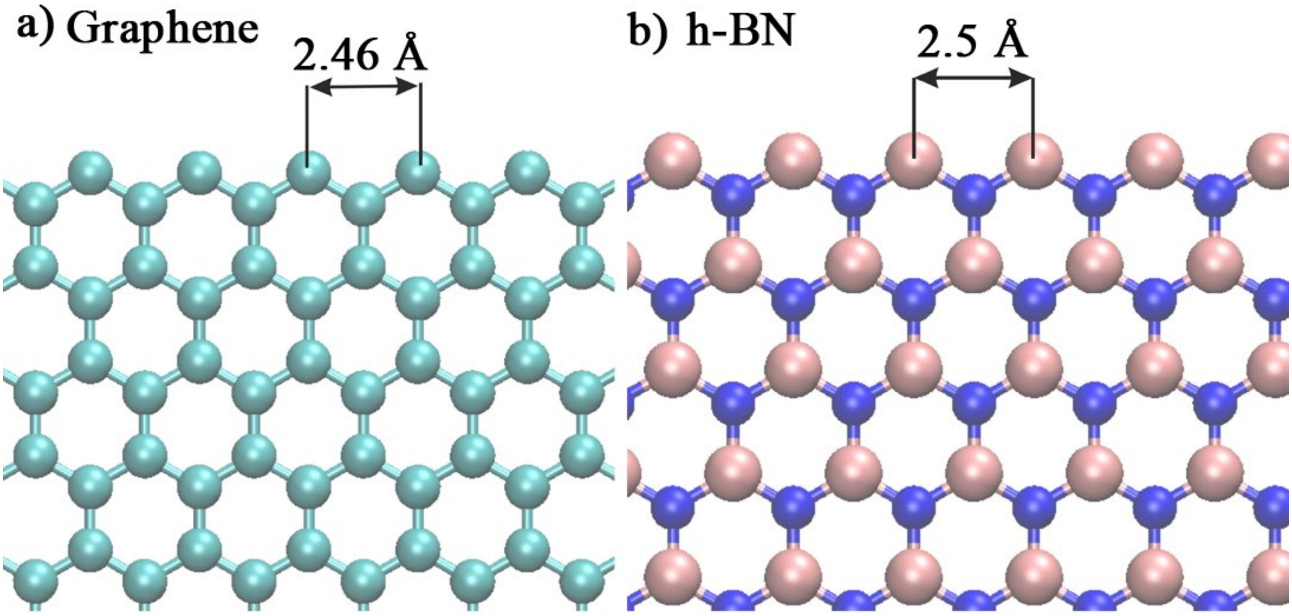

Fig. 3.3 Graphic representation of the structure of a) graphene b) h-BN substrates.

Circular shape with a radius of 200 Å and a thickness of 1 atom (Fig. 3.4) was chosen for h-BN and graphene substrates. The total number of 46 279 atoms was in the h-BN substrate and 48260 for graphene. Such a size of the substrate enables us to keep computing time reasonable. On the other hand, this number of atoms is sufficient to account for the majority of effects occurring in the system under bombardment with fullerenes.

It is known that the systems with a limited number of atoms require special care in computer simulations [15]. Proper boundary conditions must be applied in this context because the substrate waves, produced by C_{60} impact, will be reflected by the boundaries of the system toward the center of the sample. This process will generate artifacts in the simulation results. Several approaches have been suggested to minimize the effect of reflected waves [15]. The most efficient one is based on a division of the substrate into three zones with different propagation conditions of pressure waves, as shown in Figure 3.4.

The motion of atoms in the regular zone (Fig. 3.4.) is described by classical Newtonian equations of motion with no restrictions applied. The interaction of C_{60} with the substrate occurred in this zone. The second zone, which is called stochastic, surrounds the central zone. Additional restrictions to the atom motion are applied here, namely, frictional forces are introduced. These forces damp the movement of atoms proportionally to their velocities. This approach results in energy dissipation from the propagating waves in the second zone. The last zone, which is only 4 Å thick, contains rigid atoms. The role of this zone is to restrain the displacement of the whole substrate during the bombardment. The three-zone substrate was relaxed to allow atoms to occupy equilibrium positions, and afterward, it was bombarded by C_{60} projectiles with different kinetic energies and impact angles.

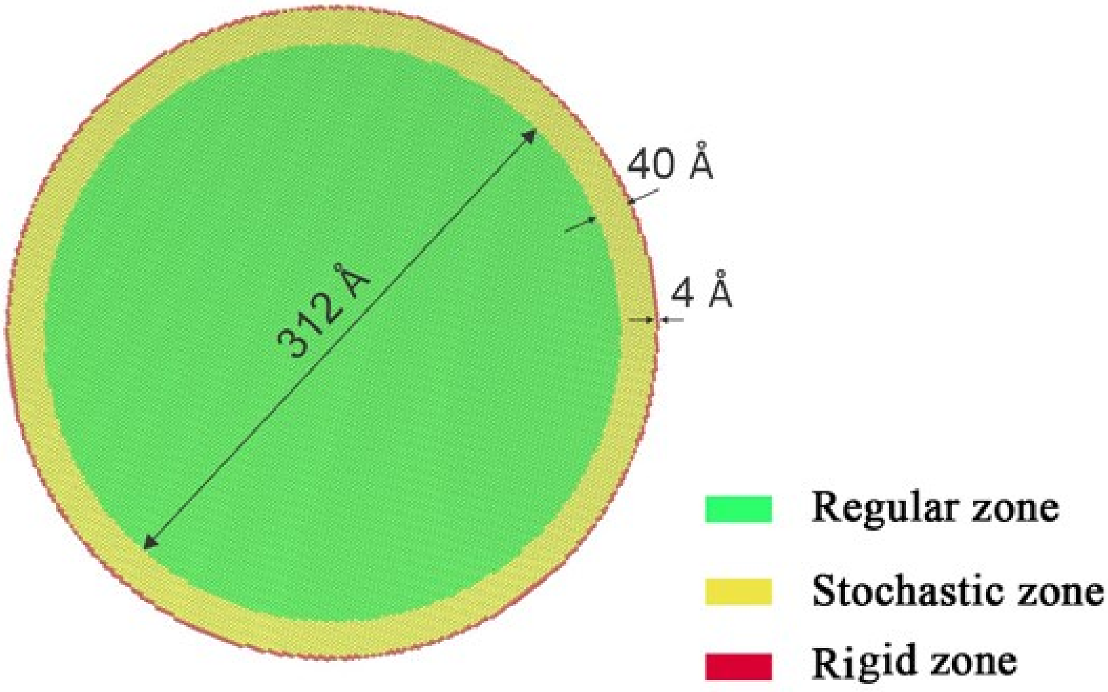

Fig. 3.4. Graphical representation of a substrate divided into three zones. The regular, stochastic, and rigid zones are marked with green yellow and red colors, respectively.

3.4. Simulation time

The simulation time should be chosen so that the system under study reaches a saturation state, which means the absence of new sputtered particles beyond the selected simulation time. Fig 3.5. shows the mass of all ejected particles vs. simulation time. The graph was constructed for the C_{60} projectile bombarding h-BN substrate at the 0.7, 10, 50, keV energy and 0°, 45°, 81° incidence angle. It is known that the saturation time depends on the energy and impact angle, therefore the energies and angles in fig. 3.4. were chosen to cover the whole range of the parameters used in the simulations.

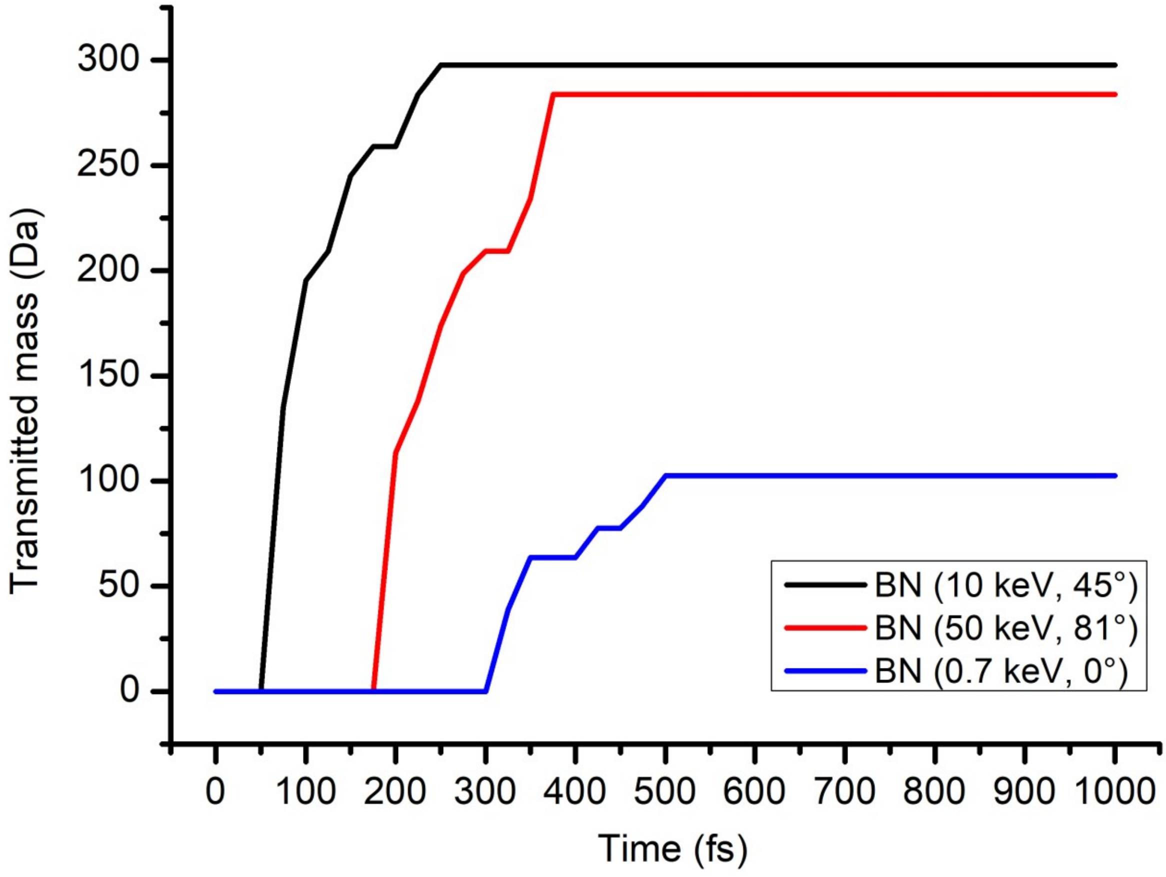

Fig. 3.4. Dependence of h-BN ejected mass vs the simulation time for 10, 50, 0.7 keV energy and 45°, 81°, 0° incidence angle, respectively.

The 10 keV energy and 45° impact angle were chosen as standard parameters for the typical simulation time. One can see (Fig. 3.4), that the saturation occurred already at 250 fs for 10 keV energy and 45° impact angle. The boundary points, which are 50 keV, 81°, and 0.7 keV, 0° require longer simulation times. The saturation occurred at 400-500 fs for these impacts. Therefore, it is safe to state that 1 ps of simulation time is sufficient to account for all transmitted particles regardless of the impact of energy and incident angle. Such simulation time is adapted in my studies.

4. Results and discussion

The main goal of the work was to compare the efficiency of the sputtering of h-BN and graphene substrates by C_{60} projectile under the same impact conditions. Therefore, the same energy, impact points, and angles were used for both systems.

4.1 Disintegration of the projectile at sputtering

The flux emitted in transmission direction contains the atoms of the projectile along with h-BN and graphene substrates atoms. The projectile atoms result from the destruction of the C_{60} in the course of the sputtering process. Their number depends on the substrate material, the impact angle, and the initial energy of C_{60}. The number of projectile atoms in the flux emitted in transmission direction was calculated for h-BN and graphene substrates. The results of the calculations are presented in Fig 4.1.

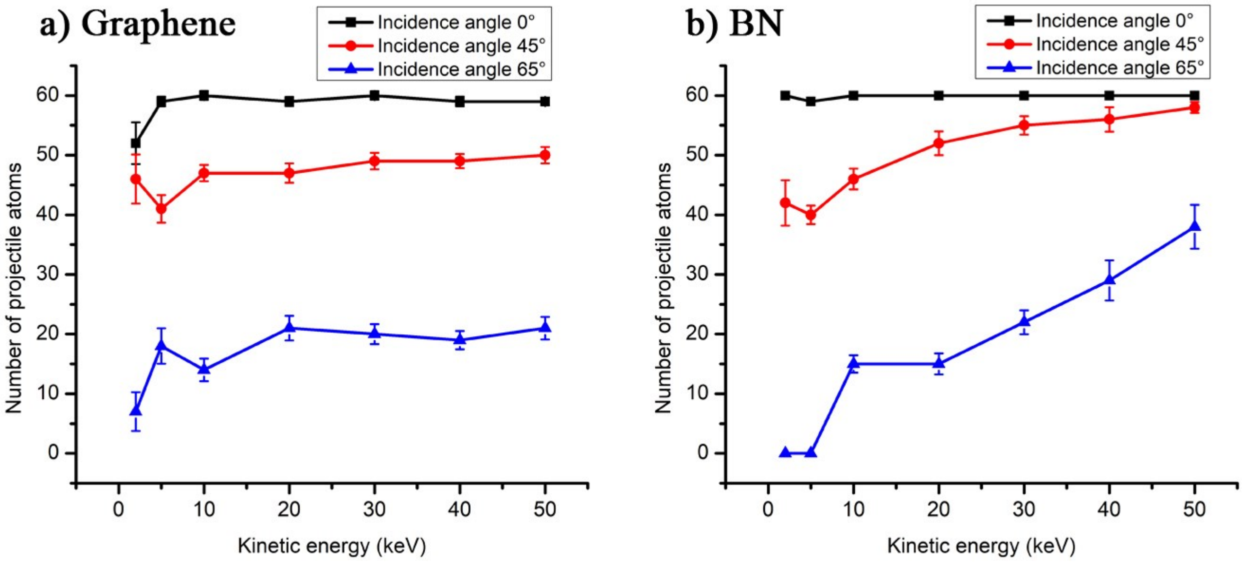

Fig. 4.1. The dependence of the number of projectile atoms in the flux emitted in transmission direction vs. the impact kinetic energy for a) graphene b) h-BN substrates. Each point in the graphs is the result of data averaging over 25 impact points at the substrates.

One can see that the number of projectile atoms in the flux emitted in transmission direction decreases with the increase in the incident angle for both graphene and h-BN substrates. The magnitude of the effect is quite similar for both investigated substrates. For example, at the impact energy of 10 keV, the number of particles B and N decreases from 60 ± 0.2 to 15 ± 1.44 with an increase of the incident angle from 0 to 65 degrees, respectively. However, the pattern of the variation differs substantially when the kinetic energy is concerned. The number of projectile atoms in the flux emitted in the transmission direction of the graphene substrate is almost independent of the C_{60} energy, slight growth is observed at low energies only. This is not the case for the h-BN substrates. In this case, gradual growth in the number of projectile atoms is observed with the increase of the kinetic energy. The sole exception is the h-BN substrate sputtered at 0 degrees. In this case, the number of projectile atoms does not depend on C_{60} energy. This is because the B-N atoms have a weaker than C-C atoms binding energy, and C_{60} projectile was intact during the sputtering of the h-BN substrate at energies 0.6-1.5 keV, which is not the case for the graphene substrate (Fig. 4.2).

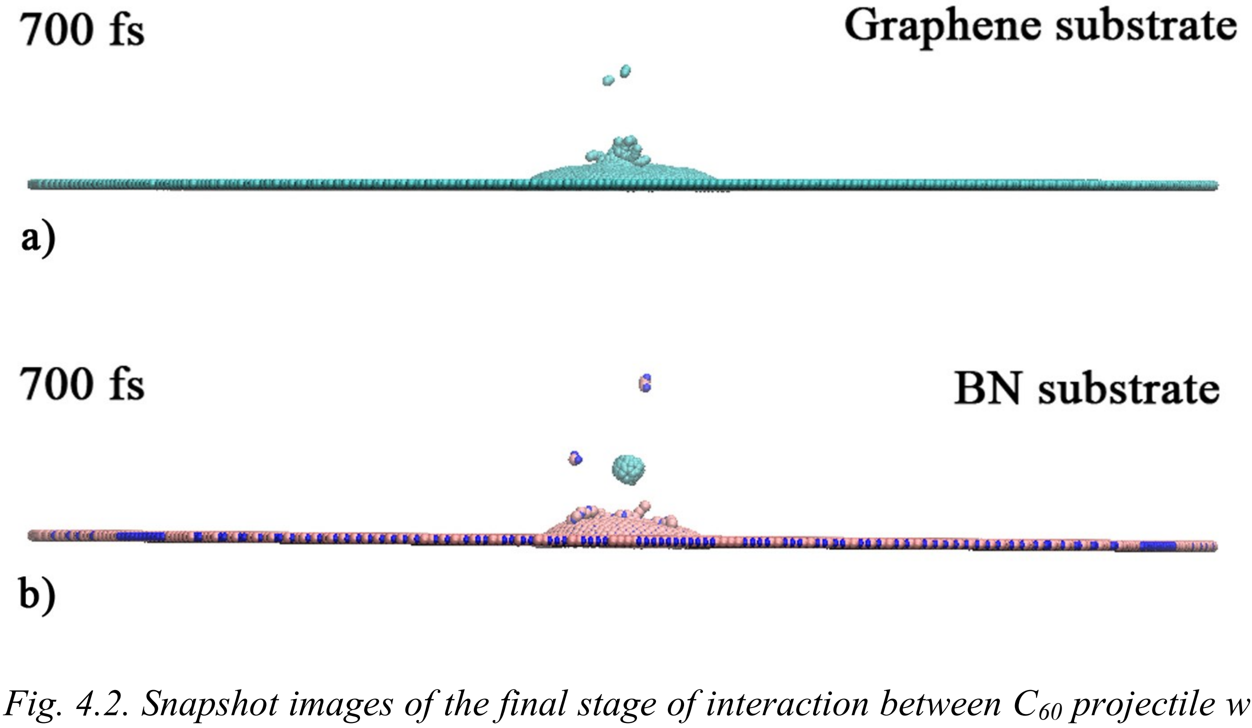

Fig. 4.2. Snapshot images of the final stage of interaction between C_{60} projectile with the energy 0.7 keV and graphene (a) and h-BN (b) substrates. Please note that C_{60} projectile was not destroyed when bombarding the BN substrate case.

Subsequently, the remain kinetic energy (after the penetration process) of the C_{60} projectile atoms was studied for graphene and h-BN substrates. The results of the calculations are summarized in Fig. 4.3.

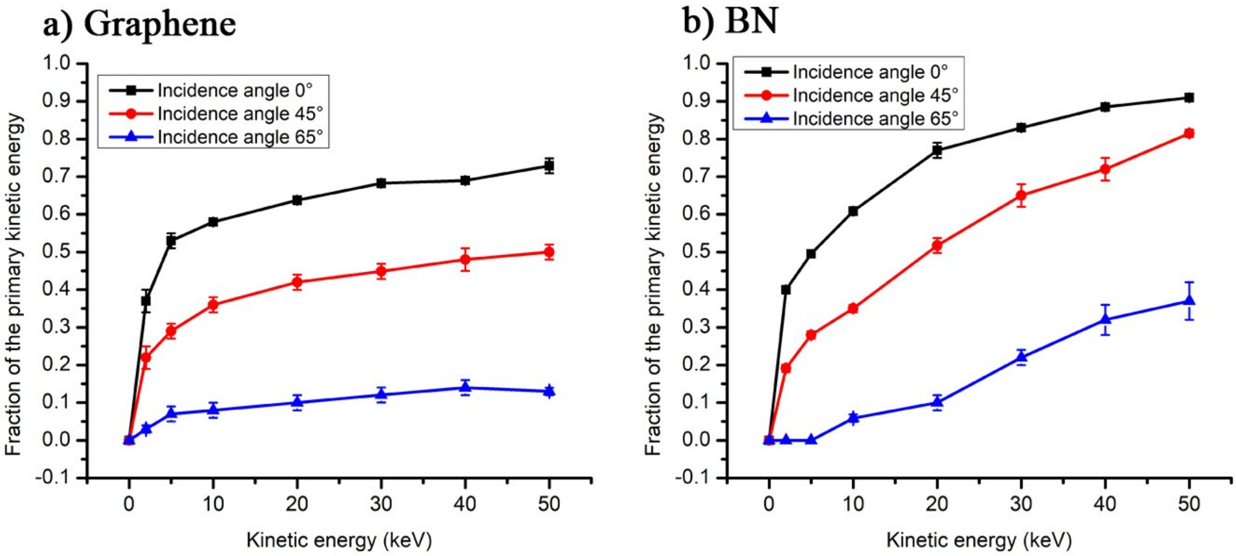

Fig. 4.3. Dependence of the transferred kinetic energy of C_{60} *projectile on the impact energy and incident angle for graphene (a) and h-BN (b) substrates. Each point in the graphs was the result of data averaging over 25 impact points of the substrates.*

One can see the substantial growth of the projectile kinetic energy in the 0 - 10 keV range followed by slight growth in the 10 – 50 keV range for the case of the graphene substrate. However, the “saturation” value greatly depends on the incident angle. Thus, the fraction of the energy of the projectile decreases from 0.75 to 0.1, with the incident angle increase from 0 to 65 degrees. In the case of the h-BN substrate, the energy of the projectile atoms gradually increases with the kinetic energy, reaching the maximum value of 90% of the primary energy at the incident angle of 0 degrees.

The observed difference in the pattern of the variation of the projectile energy (fig. 4.3) during penetration through graphene and h-BN substrates results mainly from the different binding energies of B-N (6.66 eV) and C-C (7.41 eV) atoms. This difference leads to a higher number of projectile atoms transmitted through the h-BN substrate compared to graphene counterpart at energies higher than 10 keV. As a result, transmitted C60 projectile atoms also have higher kinetic energy compared to the graphene substrate case.

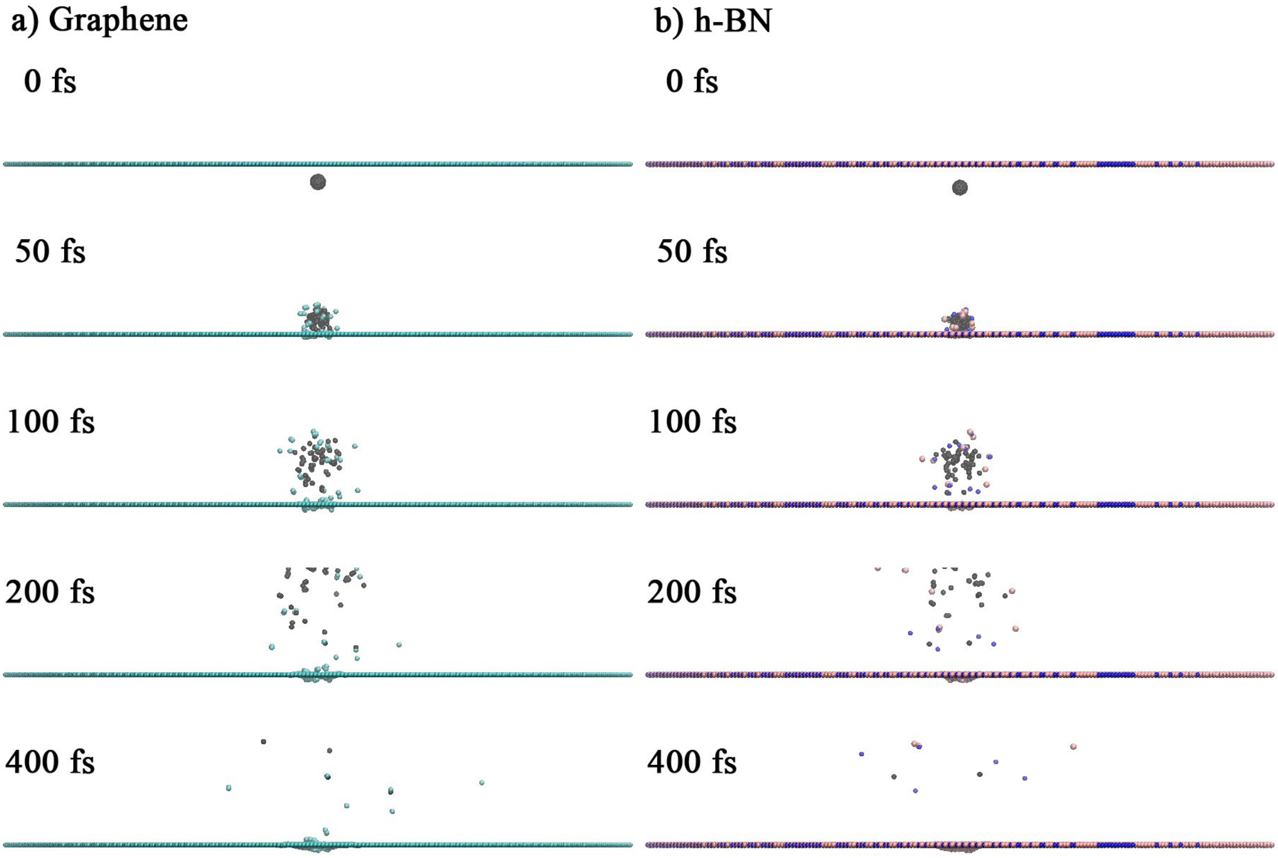

Fig. 4.4. Time sequence of stages of the sputtering process of a) graphene and b) h-BN substrates. The energy of C_{60} *was 10 keV, and the incident angle was 0°.*

One can see, that the number of penetrating C_{60} projectile atoms decreases with increasing of impact angle as it is shown in Figure 4.1. This is because the number of reflected atoms increases with the increase of impacted angle. This is clearly visible in Figures 4.4 and 4.5, which show the sputtering process for graphene and h-BN substrates for 0° and 60° of C_{60} projectile impact angles. One can see that at 0° impact angle, all projectile atoms are penetrated through substrates. In the case of 60° the large fraction of projectile atoms is reflected from the substrate.

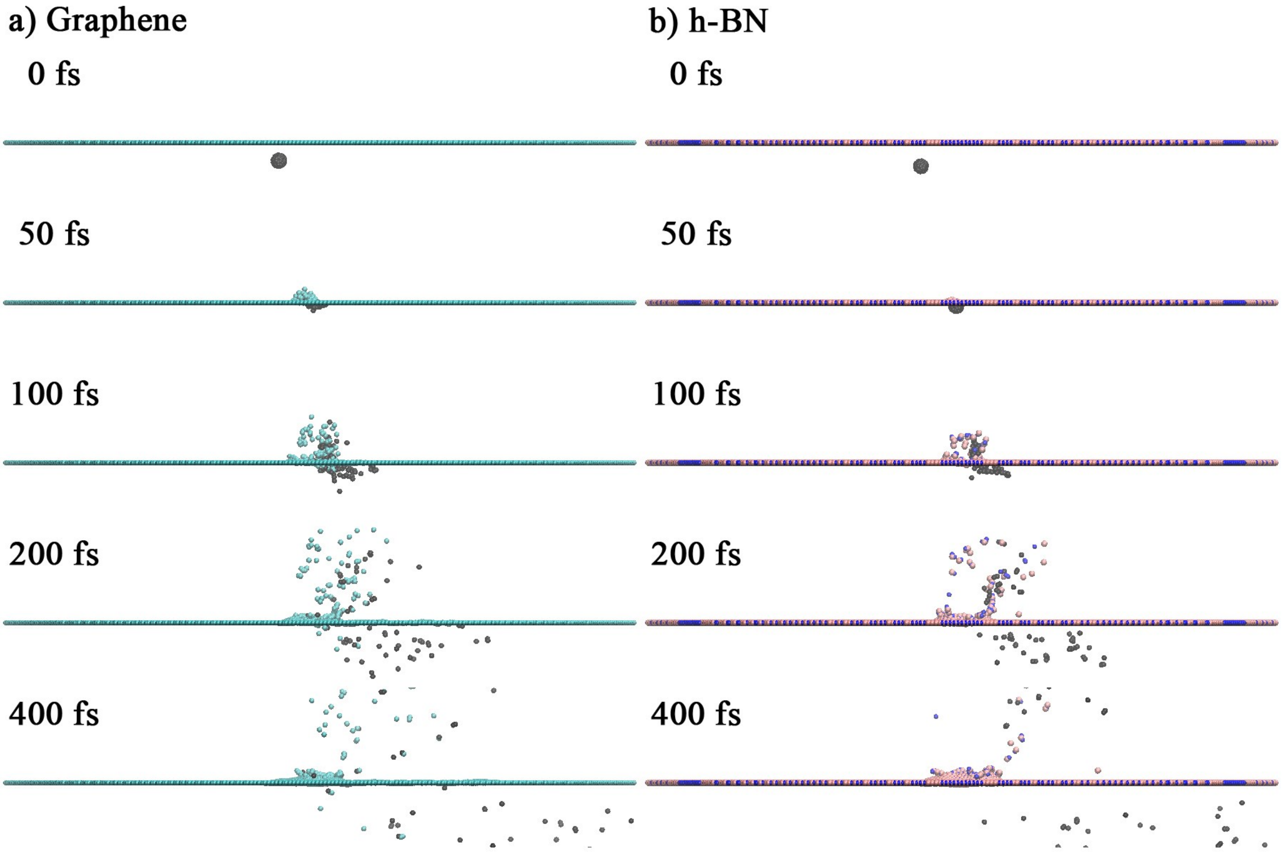

Fig. 4.5. Time sequence of stages of the sputtering process of a) graphene and b) h-BN substrates. The energy of C_{60} was 10 keV, and the incident angle was 60°.

4.2. Mass emitted in the transmitted direction of the substrate vs kinetic energy

Figure 4.6 shows the results of simulation of a mass emitted in the transmitted direction at different kinetic energies of the C_{60} projectile. The impact angle of 0° was used in the simulations. The mass emitted in the transmitted direction was used in the graphs instead of the number of transmitted atoms. This is because the flux emitted in the transmission direction contains atoms of several chemical elements. Each element is characterized by its own sputtering coefficient, therefore the measuring of the number of atoms is much less representative. As a result, the units of mass or volume are used in case of sputtering of multicomponent substrates, making possible a direct comparison between various materials. It should be noted, that the mass of C atom (12 Da) and average mass of B and N atoms (12,4) are very similar. Thus, the comparison of the sputtered mass of graphene and BN substrates is much more convenient in Da rather than in counts of atoms.

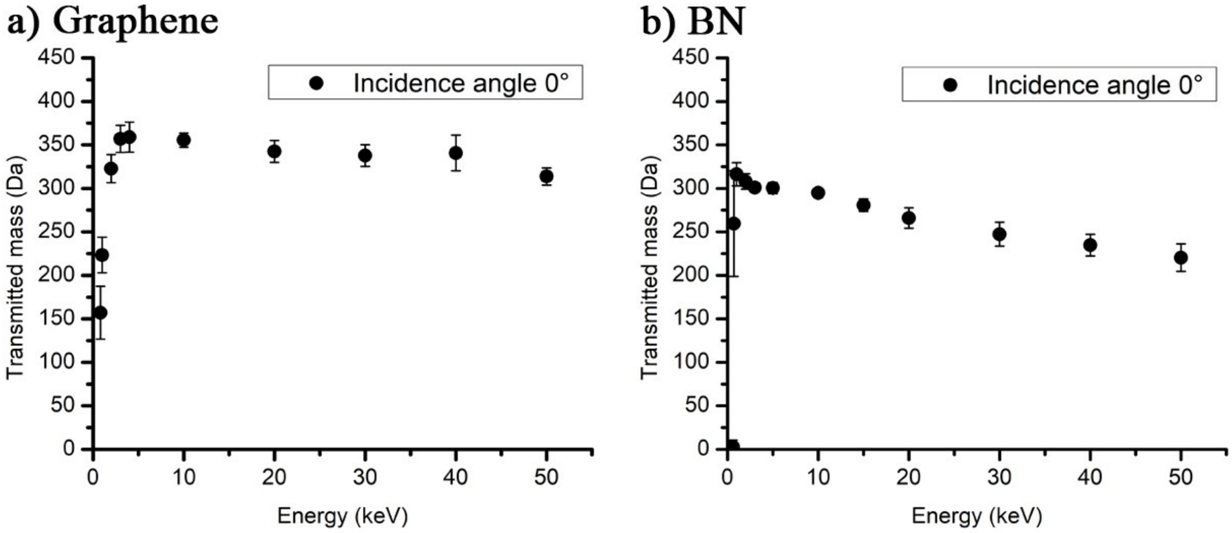

Fig.4.6. Dependence of the mass emitted in the transmitted direction of the sample on the energy of the projectile at 0 degrees impact angle for graphene and h-BN substrates.

A rapid increase in the mass emitted in the transmitted direction to a maximum value of 358 Da at 3 keV is observed for the graphene substrate case (Fig. 4.6a). At higher kinetic energies, the mass emitted in the transmitted direction gradually decreases from the maximum value to 310 Da at 50 keV. In the case of the h-BN substrate, the mass emitted in the transmitted direction also increases but reaches the maximum value already at the energy of 1 keV. The gradual decrease in the mass emitted in the transmitted direction for both substrates is visible in Fig. 4.6 with the C_{60} energy increase, and it is associated with a decrease of projectile-substrate interaction time.

The simulations showed (Fig. 4.6) that the mass emitted in the transmitted direction decreases faster for the h-BN substrate with the increase in the impact energy. This is a somewhat unexpected result. We supposed that the mass emitted in the transmitted direction should be larger for the h-BN substrate, compared to the graphene one, because the binding energy of B-N atoms (6.66 eV) is lower than the graphene one (7.41 eV). Therefore, additional studies are required for further insight.

4.3. Mass emitted in the transmitted direction vs. incident angle

Figure 4.2 shows the results of simulation of the sputtering process at different C_{60} incident angles for graphene and h-BN substrates. Three different energies of the projectile, namely 2, 10, and 50 keV were investigated.

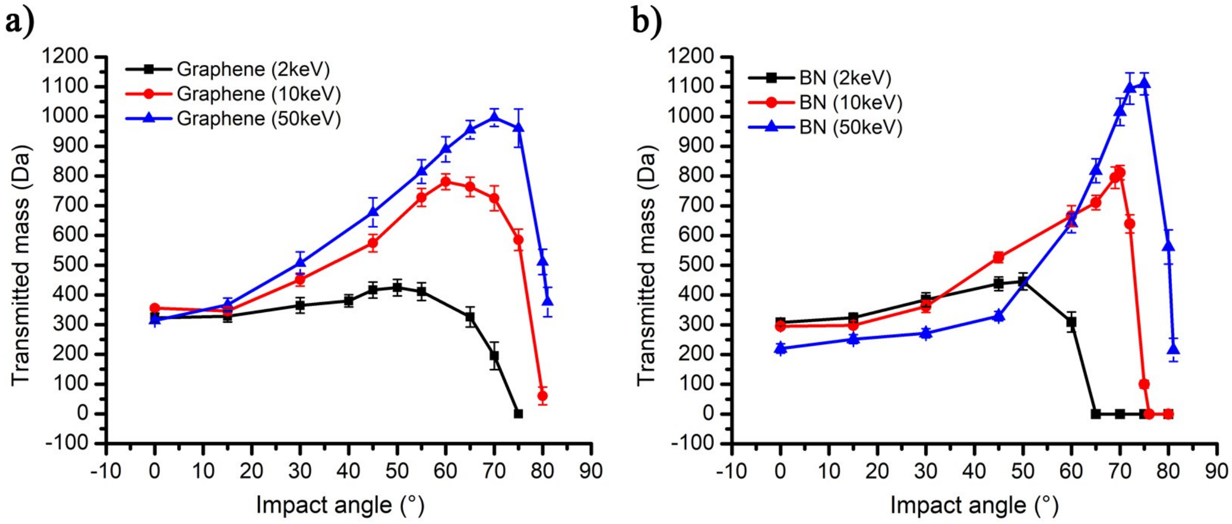

Fig. 4.7. The dependence of the mass emitted in the transmitted direction on the impact angle for 2, 10, 50 keV C_{60} projectile.

One can see that the shape of the curves representing the angular dependence of the mass emitted in the transmitted direction for graphene and h-BN substrates at 2 keV is similar. In both cases, almost no variation of the mass is observed at 0-50 degrees of the impact angles. At higher angles (50-65°), a rapid decrease in the mass emitted in the transmitted direction is clearly registered for both substrates. The major difference is observed at angles higher than 65 degrees. In that case, the h-BN substrate is not sputtered at all due to insufficient energy of the C_{60} projectile, while in the case of graphene substrate, the impact angle of 75 degrees is required to vanish the sputtering process.

The behaviour changes with the increase of the energy of the projectile to 10 keV. The mass emitted in the transmitted direction gradually increases with the increase of the impact angle and reaches the maximum value at the angle of 65 and 70 degrees for graphene and h-BN substrates, respectively. Further increase of the impact angle results in a sharp drop in the mass for both substrates. One can state the avalanche-like decrease of the mass emitted in the transmitted direction in the case of the h-BN substrate; it dropped to 0 already at 76 degrees.

A similar situation is observed for the energy of 50 keV. In both cases, the mass emitted in the transmitted direction increases with the increase of the impact angle. The mass emitted in the transmitted direction of the carbon substrate increases gradually, while the h-BN substrate transmitting mass is subject to rapid increase at angles higher than 45 degrees. Both curves reach the maximum at the angle of 75 degrees, followed by a sharp decrease at higher angles. It should be noted that the optimal angle, i.e., the impact angle resulting in the highest transmitting mass value, increases with the projectile energy increase. One can see, that the mass emitted in the transmitted direction in h-BN substrate case is ~12% larger than in the graphene case under optimal impact angle and impact energy of 50 keV. This is because the C_{60} projectile did not perforate the substrate at large impact angles, but it was reflected by the substrate, of course, transferring only a fraction of energy to the substrate. In this case, the h-BN substrate is sputtered better than graphene one (incident angles 70 degrees at 10keV, and 70-85 degrees at 50 keV), as it is visible in fig. 4.7. In these cases, the projectile transfers similar energy to both substrates. The binding energy of B-N atoms (6.66 eV) is smaller than the graphene one (7.41 eV), therefore, less energy is required to sputter the h-BN substrate, resulting in a larger number of sputtered particles. This effect exists for all energies, however, for low energy range, it is hard to observe it due to a small total yield.

The mass emitted in the transmitted direction increases with the increase of the impact angle of the projectile (Fig. 4.7). This is because with the increase of the angle, the interaction area between the substrate and the projectile also increases (Fig 4.8). Thus, the hole in the substrate and the total yield increase too [16]. It should be noted, that the total yield reaches its maximum at some angle. The further increase of the impact angle leads to a significant decrease of the substrate hole and total yield (Figs. 4.7, 4.8). One can see, that this angle depends on projectile energy and substrate materials (Fig. 4.7).

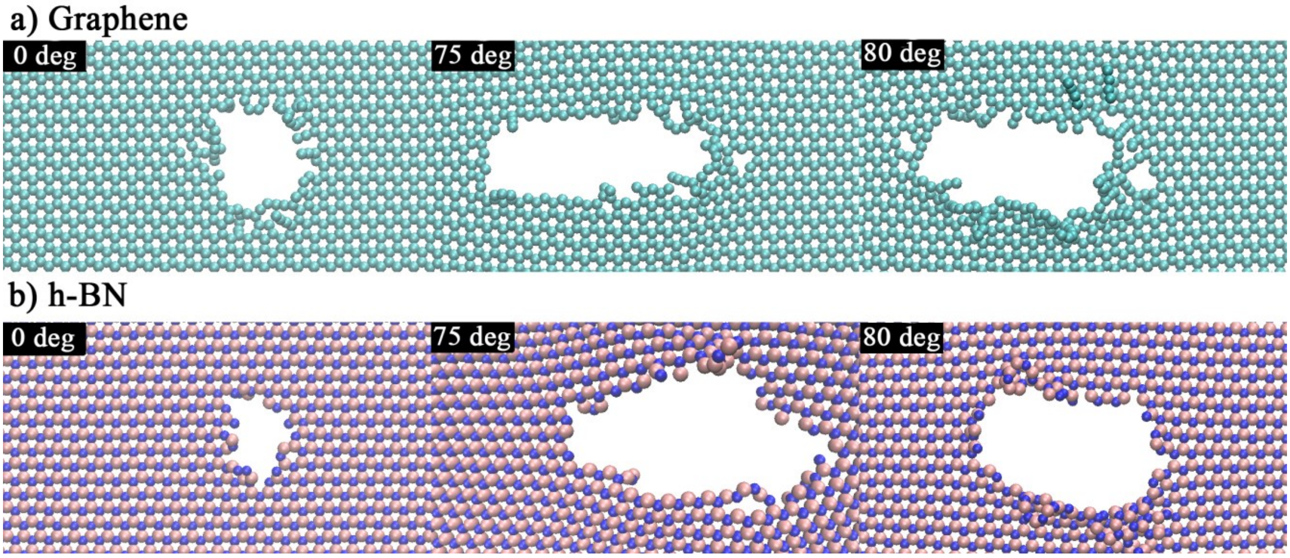

Fig. 4.8. Size of the hole in the graphene (a) and h-BN (b) substrates at different impact angles (shown in the left upper corner). The impact energy of C_{60} projectile 50 keV was used.

4.4 Angular dependence of the sputtered mass.

The substrate layer is destroyed under a bombardment with the high-energy C_{60} projectile. As a result, the substrate atoms are ejected of both sides of the substrate, i.e., there are atoms ejected along the direction of projectile motion, and the atoms ejected in the backward direction. Such particles were counted too, and the variation of the sputtered mass versus the incident angle is presented in Fig. 4.9.

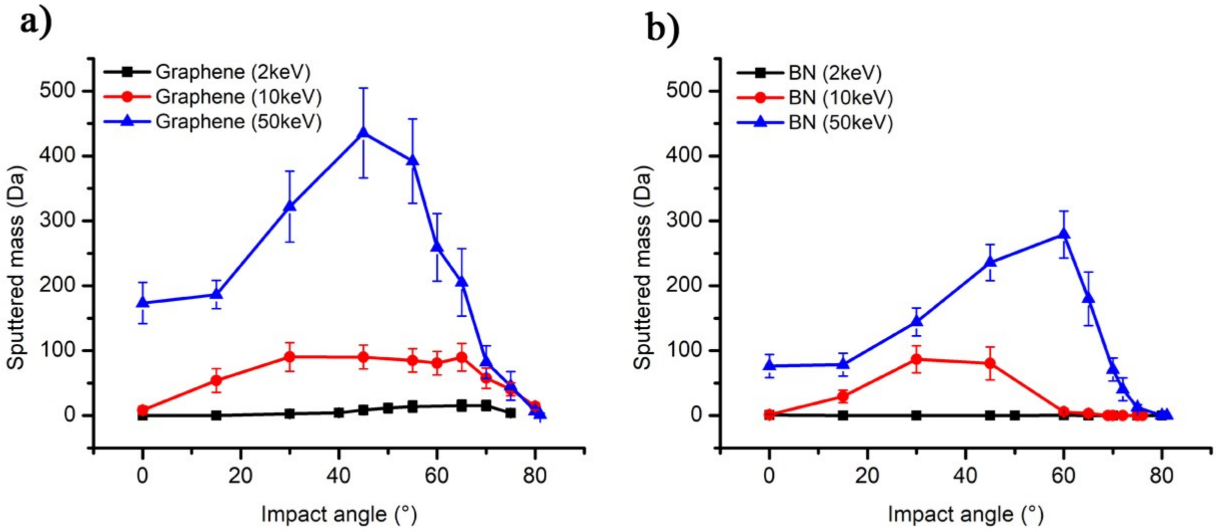

Fig. 4.9. The dependence of sputtered mass on the impact angle for 2, 10, 50 keV incident energy of C_{60} projectile bombarding a) graphene and b) BN sample.

One can see that the amount of the sputtered mass is almost zero regardless of the impact angle for both substrates for the bombardment energy of 2 keV. This is because the impact energy 2 keV is too low for sputtering a noticeable number of particles. The increase of the projectile energy to 10 keV results in the appearance of the sputtered particles, however, their number is not significant, and their total mass did not exceed the value of 100 Da for both substrates. The situation changes the projectile impact energy 50 keV. The sputtered mass in the case of the graphene substrate significantly exceeds the one for the h-BN substrate at all incident angles. However, the shape of the signal vs. impact angle is similar to both substrates. The maximum value is observed at 45 and 60 degrees for graphene and h-BN, respectively. The number of sputtered particles depends on the energy transferred to the substrate by C_{60} projectile. Figure 4.3 shows, the fraction of the remaining energy of projectile atoms was higher for the h-BN substrate case, as compared with the graphene case. Thus, the graphene substrate absorbs more energy from C_{60} projectile. As a result, a significant increase of the mass emitted in the sputtering direction occurs at high impact energies. Consequently, a larger mass was emitted in the sputtering direction in the graphene substrate case compared to h-BN counterpart at 50 keV impact energy (Fig. 4.9).

The factors affecting the shape of the graphs shown in Figure 4.9 are similar to those of the case of particles emitted in the transmitted direction, which were described in detail in section 4.3.

4.5 Mass analysis

Figures presented so far were focused on a total mass of ejected species. No information about the mass distribution of emitted particles was given. To address this issue, the mass spectra of sputtered products were calculated for graphene and h-BN substrates bombarded by C_{60} projectile at 2, 10 and 50 keV energies and 0° and 45° impact angles.

Figures 4.10, 4.11 and 4.12 show mass spectra resulted from the bombardment of graphene and h-BN substrates. It should be noted, that all mass spectra presented in the study were produced by averaging data from 25 points bombarded by C_{60} projectile. One can see, that the emission of bounded atoms dominates in the flux emitted in transmission direction at low energies of the projectile (2 keV in this case), as it is shown in Fig 4.10.

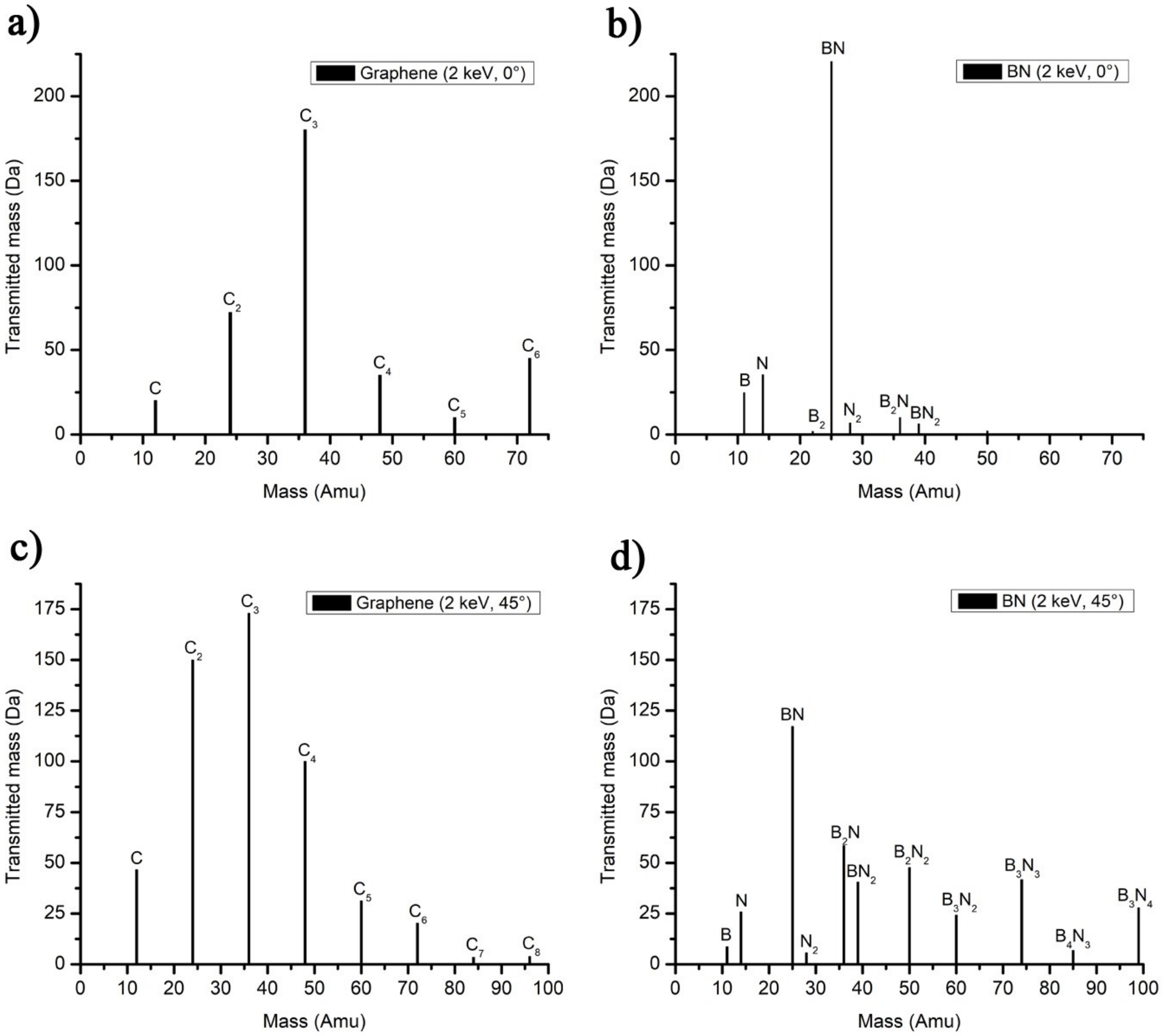

Fig. 4.10. Mass spectra for graphene and h-BN single layer substrates at 2 keV C_{60} projectile and 0° and 45° impact angles.

The size of the ejected clusters increases with the angle increase. This trend is the same for all energies studied. One can see that for 10 keV impact energy, the size of the ejected clusters significantly decreases (Fig. 4.11). It should also be noted, that the number of ejected clusters significantly decreases for both substrates too.

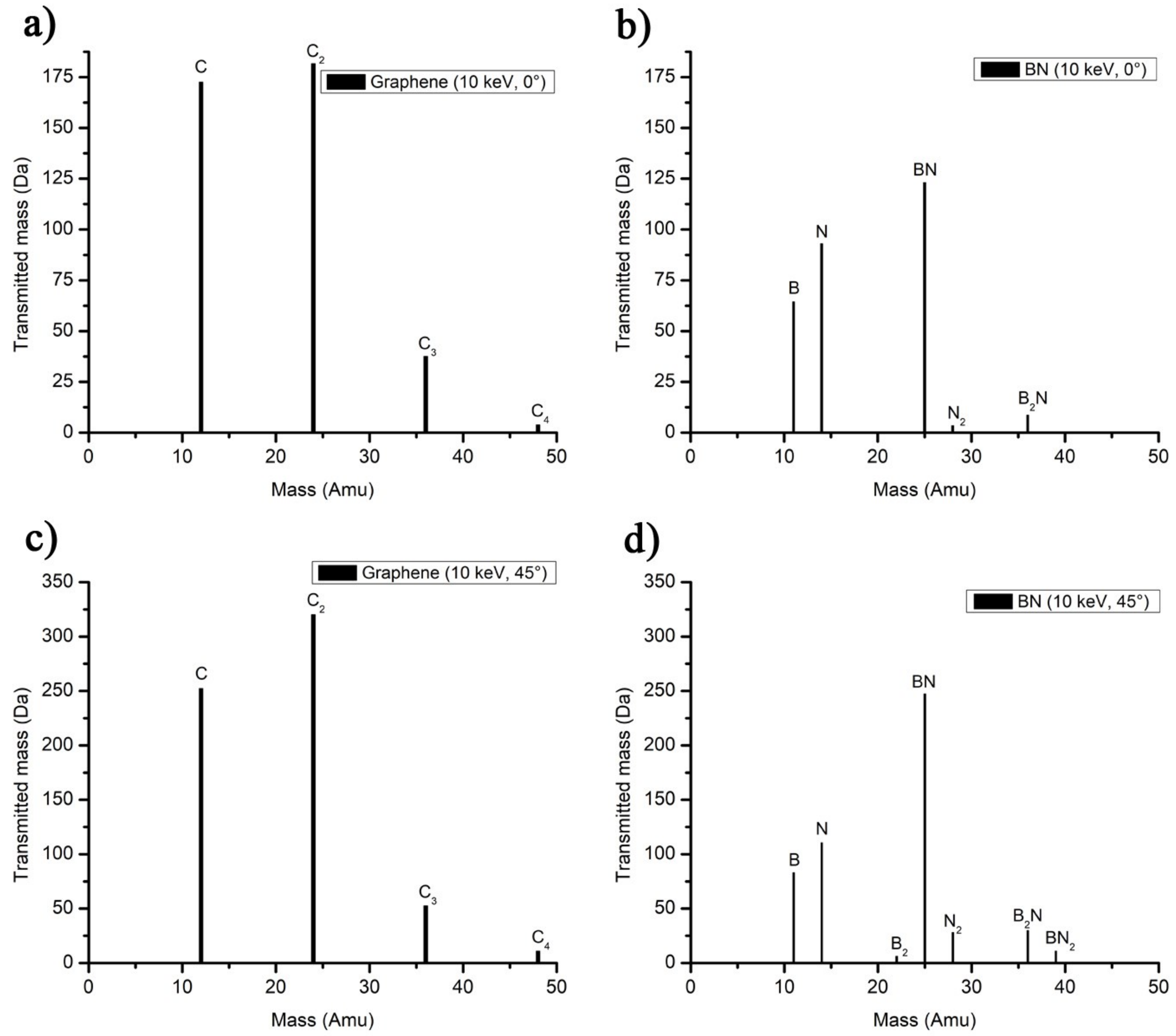

Fig. 4.11. Mass spectra for graphene and h-BN single layer substrates for 10 keV energy and 0° and 45° impact angles.

One can see that most of the clusters were destroyed at the energy of 50 keV (Fig. 4.12). All bindings between B and N atoms were destroyed for h-BN substrate at the incident angle of 0° (Fig. 4.12b), however, several molecules survived at 45° (Fig. 4.12d). It should be noted that almost all bindings were destroyed for the C substrate at 50 keV too (Fig. 4.12 a, c).

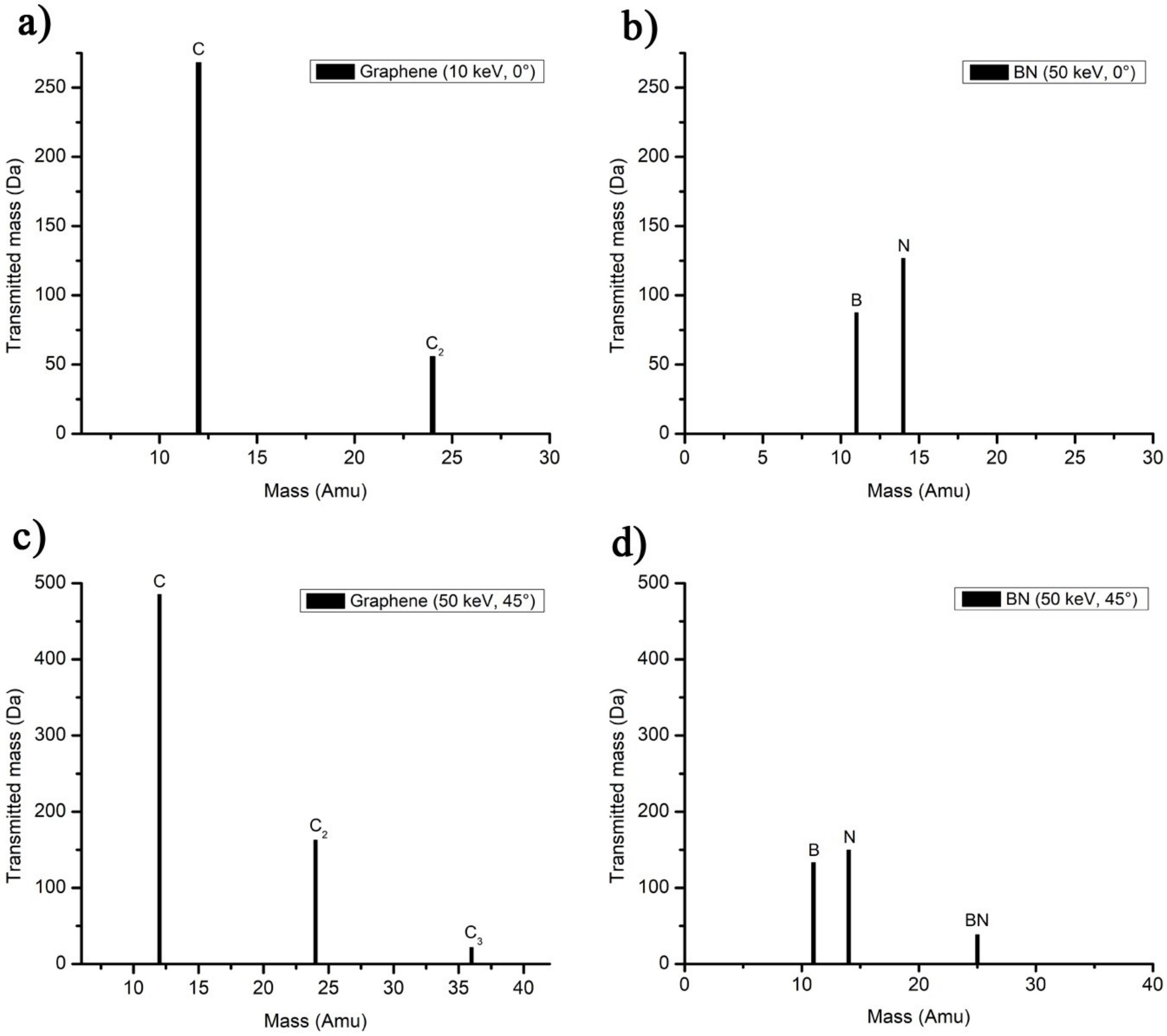

Fig. 4.12. Mass spectra for graphene and h-BN single layer substrates at the incident energy of 50 keV and impact angles 0° and 45°.

In summary, both the kinetic energy and the impact angle strongly affect the composition of the mass emitted in the transmitted direction. The number and size of ejected clusters decrease with the energy increase. The fragmentation strongly decreases with the impact angle increase. We believe that the number of bounded atoms depends on the binding energies, and this energy is higher for the graphene substrate, therefore more energy is required for its destruction.

4.6 Organic particles emission

The efficiency of the ejection of organic particles strongly depends on the substrate, they are deposited on. One of the most important parameters, which influences the emission of organic particles is the substrate bending under the bombardment. This is due to the ejection of organic molecules from the substrate by “Trampoline” effect [1].

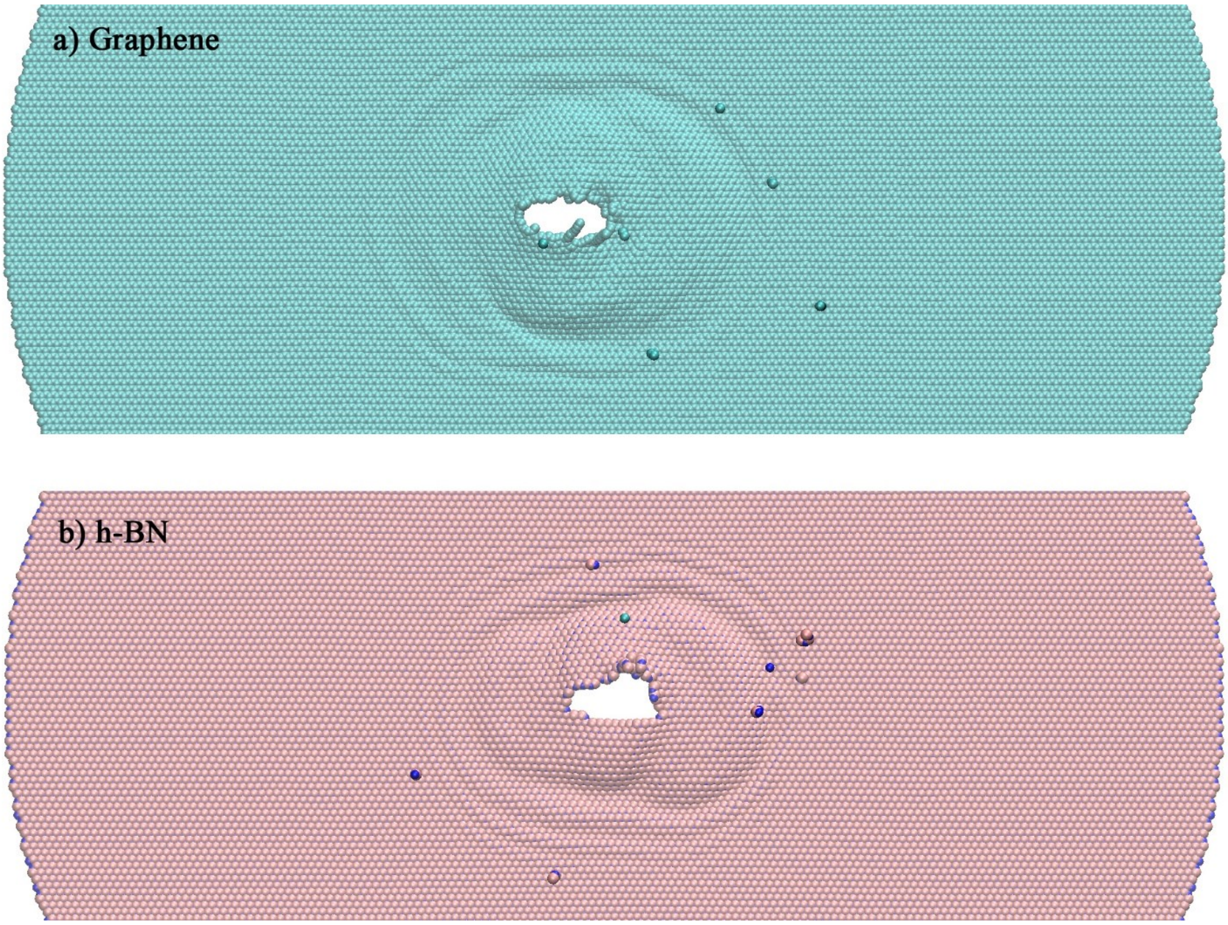

Fig. 4.13. Top view of the substrate bending under bombardment by C60 projectile (50 keV impact energy and 75° impact angle). a) is graphene and b) is h-BN substrates

Figures 4.13 and 4.14 present top and side view of graphene and h-BN substrates under bombardment by C60 projectile. One can see, that the bending area is very similar for both substrates (fig. 4.13). Please also note that the degree of bending is similar for these substrates too (fig. 4.14). This is because the Young module of h-BN monolayer is the same order of magnitude as the graphene one, only a 13% difference is observed. Thus, the Young module of h-BN is 0.865 TPa, while the graphene one is 1 TPa, according to data of Ref. [14]. Therefore, no significant difference in the emission of organic molecules is expected for these substrates.

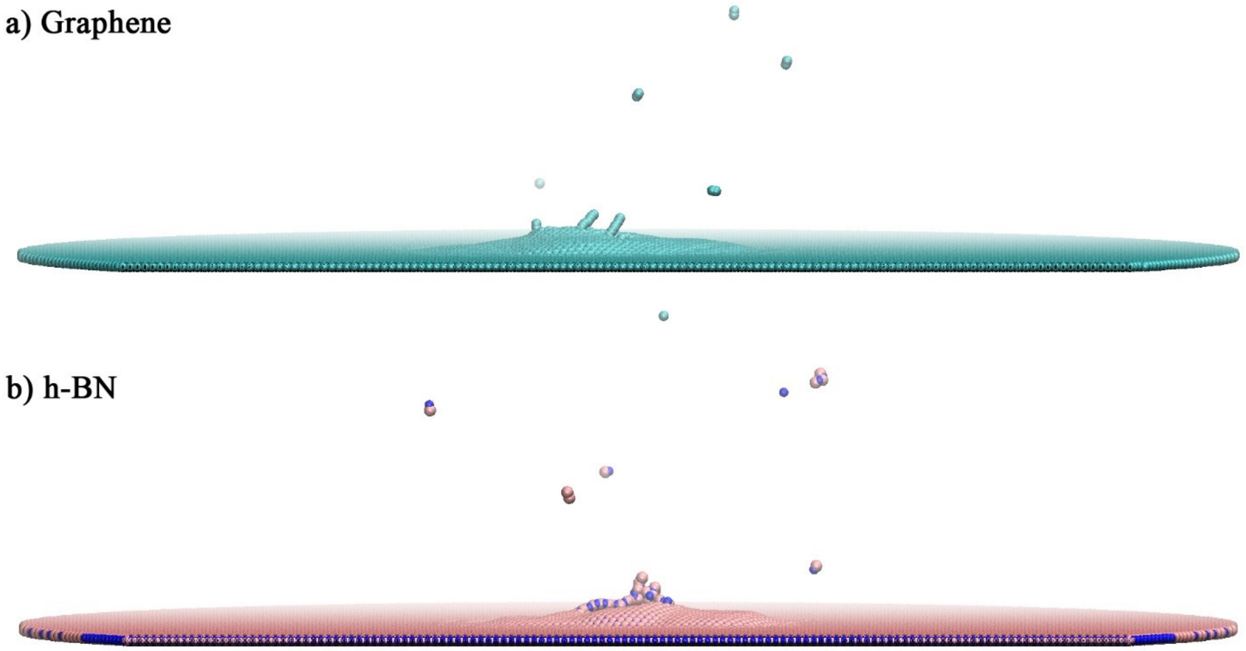

Fig. 4.14. The side view of the substrate bending under bombardment by C60 projectile (50 keV impact energy and 75° impact angle). a) is graphene and b) is h-BN substrates

5. Summary

The simulation of the sputtering process of graphene and h-BN single layer substrates by C_{60} fullerene molecule has been carried out by means of molecular dynamics in a wide range of impact energies and angles. The main results are:

- The h-BN substrate is sputtered better than graphene one in the case C_{60} projectile is not transmitted but reflected from the substrate. This is true for all energies used in the study.
- The sputtered mass increases with the increase of impact angle, which is related to the increase of the interaction area [16]. The sputtered mass reaches the maximum value at some impact angle, which could be considered as the optimal angle. The optimal angle value depends on the projectile energy and the substrate material.
- It has been shown that the C_{60} projectile did not disintegrate during the sputtering of the BN substrate with the impact energy 0.6-1.5 keV. Sputtering of the graphene substrate results in the disintegration of the C_{60} projectile regardless of the impact energy. This is explained by the difference in the binding energies of B-N (6.66 eV) and C-C (7.41 eV) atoms.
- The mass emitted in the transmitted direction of the h-BN and graphene substrates were similar under the majority of bombardment parameters used in the study. The simulations showed that the mass emitted in the transmitted direction decreases faster for the h-BN substrate case with the increase in the impact energy at 0° impact angle. This result is somewhat unexpected because the binding energies of B-N atoms are weaker than C-C ones, and the h-BN substrate should be sputtered better than graphene one at the conditions. Therefore, additional studies are required for further insight.
- The bending area and the bending degree of graphene and h-BN substrates were similar under bombardment by C_{60} projectile

Based on the performed simulations, one can speculate that an organic layer will not be sputtered substantially better on the h-BN substrate compared to the graphene one under similar bombardment parameters of C_{60} projectile. Indeed, the main parameters for effective transmitting of organic layers are the number of sputtering particles of the substrate and the degree of substrate bending. The sputtering yield of an organic layer directly depends on the mass emitted in the transmitted direction of the substrate [16]. This mass might be slightly greater (up to 12%) for the h-BN substrate case at optimal impact angles. On the other hand, the degree of bending is rather similar for both substrates, resulting in a similar trampoline effect [1, 16]. Nevertheless, further studies of the sputtering of organic layers are required. In summary, no significant improvement in the sputtering of an organic layer deposited on the h-BN monolayer is expected compared to the graphene counterpart.

6. Literature

1. S. Verkhoturov, M. Gołuński, D. Verkhoturov, S. Geng, Z. Postawa, and E. Schweikert, "Trampoline" Ejection of Organic Molecules from Graphene and Graphite via keV Cluster Ions Impacts, J. Chem. Phys. 148, 144309 (2018)
2. M. Golunski and Z. Postawa, Effect of Sample Thickness on Carbon Ejection from Ultrathin Graphite Bombarded by keV C_{60}, Acta Phys. Pol. A 132 (2), 222-224 (2017)
3. S. Plimpton, Fast Parallel Algorithms for Short-Range Molecular Dynamics Comput. Phys. 117, 1−19 (1995)
4. R. G. Wilson, F. A. Stevie, and C. W. Magee, Secondary Ion Mass Spectrometry, John Wiley and Sons, 1989
5. J. P. Hofmann, M. Rohnke and B. M. Weckhuysen, Recent advances in secondary ion mass spectrometry of solid acid catalysts: large zeolite crystals under bombardment, Phys. Chem. Chem. Phys. 16, 5465 (2014)
6. A.W. Czanderna and David M. Hercules. Ion Spectroscopies ForSurface Analysis, volume 2 of Methods of Surface Characterization. Plenum Press, New York, 1991.
7. M. Golunski, S.V. Verkhoturov, D.S. Verkhoturov, E.A. Schweikert, Z. Postawa, Effect of substrate thickness on ejection of phenylalanine molecules adsorbed on free-standing graphene bombarded by 10 keV C_{60}, Nuclear Instruments and Methods in Physics Research B, 393, 13–16 (2017)
8. Michael P. Allen, Introduction to Molecular Dynamics Simulation, NIC Series, 23, 1-28 (2004).
9. J. H. Los, J. M. H. Kroes, K. Albe, R. M. Gordillo, M. I. Katsnelson, and A. Fasolino, Extended Tersoff potential for boron nitride: Energetics and elastic properties of pristine and defective h-BN, Phys. Rev. B 96, 184108 (2017)
10. J. F. Zieglera, M. D. Zieglerb, J. P. Biersackc, SRIM-The Stopping and Range of Ions in Matter, Nuclear Instruments and Methods in Physics Research, Section B: Beam Interactions with Materials and Atoms, 268, 1818-1823 (2010)

11. S. J. Stuart, A. B. Tutein, and J. A. Harrison, A reactive potential for hydrocarbons with intermolecular interactions, J. Chem. Phys 112, 6472 (2000)
12. M. S. Stave, D. E. Sanders, D. E. Raeker, A. E. DePristo, Corrected effective medium method. V. Simplifications for molecular dynamics and Monte Carlo simulations, J. Chem. Phys. 93, 4413 (1990)
13. S. Geng, S. V. Verkhoturov, M. J. Eller, S. Della-Negra, and E. A. Schweikert, The collision of a hypervelocity massive projectile with free-standing graphene: Investigation of secondary ion emission and projectile fragmentation, J. Chem. Phys. 146, 054305 (2017)
14. A. Falin, Q. Cai, E.J.G. Santos, D. Scullion, et al., Mechanical properties of atomically thin boron nitride and the role of interlayer interactions, Nat. Commun. 8, 15815 (2017)
15. Z. Postawa, B. Czerwinski, M. Szewczyk, et al., Enhancement of Sputtering Yields Due to C60 versus Ga Bombardment of Ag{111} As Explored by Molecular Dynamics Simulations, Anal. Chem. 75, 4402 (2003)
16. M. Golunski, Z. Postawa, Effect of kinetic energy and impact angle on carbon ejection from a free-standing graphene bombarded by kilo-electron-volt C_{60}” Journal of Vacuum Science & Technology B 36, 03F112 (2018)